Journal of Industrial and Engineering Chemistry 63 (2018) 191–200

Contents lists available at ScienceDirect

Journal of Industrial and Engineering Chemistry

journal homepage: www.elsevier.com/locate/jiec

Effect of non-covalent interactions on molecular stacking and photovoltaic properties in organic photovoltaics

Seung Jun Nam, Sung Jae Jeon, Yong Woon Han, Doo Kyung Moon*

Department of Materials Chemistry and Engineering, Konkuk University, 1 Hwayang-dong, Gwangjin-gu, Seoul 143-701, Republic of Korea

ARTICLE INFO

Article history:
Received 16 December 2017
Received in revised form 7 February 2018
Accepted 12 February 2018
Available online 21 February 2018

Keywords:
Organic photovoltaics (OPVs)
Non-covalent interaction
Face-on orientation
Dithienophenazine (DTPz)
Benzothiadiazole (BT)

ABSTRACT

The conjugated structures of donor–acceptor (D–A) type with sulfur (S), nitrogen (N) and oxygen (O) atoms aid to close packing each other in the backbone by non-covalent interactions. Furthermore, non-covalent interactions are exerted three dimensionally and affect various properties. To know this effects, we introduced different S, N and O contents as benzothiadiazole (BT) and dithienophenazine (DTPz, up or down direction of S) units on each polymer backbone. Among the three polymers, P2 with up direction of S showed an open-circuit voltage (Voc) of 0.90 V, fill factor (FF) of 54.7% and reached best power conversion efficiency (PCE) of 4.8%.
© 2018 The Korean Society of Industrial and Engineering Chemistry. Published by Elsevier B.V. All rights reserved.

Introduction

Organic photovoltaics (OPVs) have been spotlighted as green energy sources because they have advantages such as light weight, solution processability, low cost and flexibility [1,2]. The recently recorded highest efficiency of OPVs was 11.4% [3]. To enhance the efficiency of OPVs, formation and separation of the exciton are important. Thus, various studies have been conducted to modify the structures of π-conjugated polymers [4,5]. Through these structural changes, physical and optical properties of photo-active materials can be refined.

A typical method for fabricating the active layer of OPVs is the bulk heterojunction (BHJ) system, where a polymer (as a donor) is blended with a fullerene derivative (as an acceptor). The BHJ system can enhance the separation of excitons through an interpenetrating network [6–8]. The representative polymer design is the donor–acceptor (D–A) type wherein the electron donating unit (D) and the electron accepting unit (A) are alternately copolymerized. In this design, the selection of appropriate donor and acceptor building blocks can change the absorption area, energy level and packing properties [9–11].

Common donor units that have structural symmetry are widely used. Typically, there are benzo[1,2-b;4,5-b′]dithiophene (BDT) [12], indacenodithiophene (IDT) [13,14]. By contrast, asymmetrical donor units can improve the short-circuit current density (Jsc) by increasing the contact area with the PCBM derivatives. In our recent studies, we used benzo[2,1-b;3,4-b′]dithiophene (BDP), a structural isomer of BDT, to study the properties of an asymmetrical donor unit. The BDP-based polymers had high hole mobility and form a planar structure when it is copolymerized with asymmetrical acceptor benzothiadiazole (BT) unit [15].

Not only BT [16] but also phenazine (Pz) derivatives [17,18] have been studied as asymmetrical acceptors. Both units are widely used as electron accepting units because of their high electron-withdrawing properties. Specifically, Pz unit has an extended conjugated system with a stabilized structure that can lower the highest occupied molecular orbital (HOMO) levels of polymers. Also thiophene spacer was introduced to reduce steric hindrance of the polymers, and conjugation was extended by using the D–π–A system [19,20]. In such a structure, the chains of the donor and acceptor unit are arranged in the opposite direction of each other. In the previous study, we synthesized a copolymer of BDP-DTPz with planar curvature through the introduction of thiophene spacer [20.5]. Thus, we expect the BDP-π-asymmetrical acceptor type polymer backbones to be structurally stable.

Compared to the BT unit as asymmetrical acceptor, the dithienophenazine (DTPz) units had an extended conjugation structure like a Pz unit wherein the number of S atoms is increased than BT and Pz units [21–23]. Thus, this structures allow for the absorption of longer-wavelength solar light and fabrication of low

* Corresponding author.
E-mail address: dkmoon@konkuk.ac.kr (D.K. Moon).

https://doi.org/10.1016/j.jiec.2018.02.015
1226-086X/© 2018 The Korean Society of Industrial and Engineering Chemistry. Published by Elsevier B.V. All rights reserved.

band-gap polymers [24,25]. Furthermore, fused aromatic units reduce steric hindrance compared to the quinoxaline (Qu) unit and improve packing property [26].

Putta et al. studied that hetero-aromatic units simultaneously contain a weakly polar sulfur (S) and strongly polar oxygen (O) on the backbone [27]. These monomers could link to another monomer, due to the difference in electronegativity between the two atoms [28,29]. Thus, the DTPz units had a reduced molecular stacking due to non-covalent interactions. We applied this result to polymers, expecting the effective separation of electron–hole pairs.

Mondal et al. studied that a thiophene-fused unit was introduced onto the upper position of the acceptor [30]. They make two isomers, first one was the S atom pointing away from the main chain of the polymer (named Up polymer) and the other one was the S atom facing toward the main chain of the polymer (named Dn polymer). The position of the S atom affected organic solvent solubility, photo absorption and packing properties. Eventually they showed different results about mobility of electrons and power conversion efficiency.

This study prepared three conjugated copolymers based on BDP to observe the effects of non-covalent interactions such as hydrogen-bonding and chalcogen bonding between polymer backbones. The introduction of the DTPz derivatives as an acceptor extended the photo-absorption spectrum more than the BT unit and enhanced face-on packing properties of polymers layer by layer. Furthermore, the increased Jsc, due to closer molecular stacking, enhanced the efficiency of OPVs.

Experimental

Measurements

The ^{1}H NMR (400 MHz) spectra were recorded using a Brüker AMX400 spectrometer in $CDCl_3$, and the chemical shifts were recorded in units of ppm with TMS as the internal standard. Elemental analysis (EA) was performed with a Thermofinnigan EA2000. HRMS spectrometry (LC-HRMS) was recorded on a LXQ Spectrometer (Thermo Scientific) operating on ESI-TOF (MeOH as a solvent). The absorption spectra were recorded using an Agilent 8453 UV–visible spectroscopy system. The solutions that were used for the UV–visible spectroscopy measurements were dissolved in chloroform ($CHCl_3$) at a concentration of 15 μg/mL. The films were drop-coated from the $CHCl_3$ solution onto a quartz substrate. All of the GPC analyses were carried out using $CHCl_3$ as the eluent and polystyrene standard as the reference. The TGA measurements were performed using a TG 209 F3 thermogravimetric analyzer. The cyclic voltammetry (CV) were measured using a Zahner IM6eX electrochemical workstation with a 0.1 M acetonitrile (substituted with nitrogen for 30 min) solution containing tetrabutylammonium hexafluorophosphate (Bu_4NPF_6) as the electrolyte at a constant scan rate of 50 mV/s. ITO, a Pt wire, and silver/silver chloride [Ag in 0.1 M KCl] were used as the working, counter, and reference electrodes, respectively. The electrochemical potential was calibrated against Fc/Fc+. The HOMO levels of the polymers were determined using the oxidation onset value. Onset potentials are values obtained from the intersection of the two tangents drawn at the rising current and the baseline changing current of the CV curves. The lowest unoccupied molecular orbital (LUMO) levels were calculated from the differences between the HOMO energy levels and the optical band-gaps, which were determined using the UV–vis absorption onset values in the films. The current density–voltage (J–V) curves of the photovoltaic devices were measured using a computer-controlled Keithley 2400 source measurement unit (SMU) that was equipped with a Class A Oriel solar simulator under an illumination of AM 1.5 G (100 mW/cm^2). Topographic images of the active layers were obtained through atomic force microscopy (AFM) in tapping mode under ambient conditions using a Seiko SPA-300HV system at room temperature.

Photovoltaic cell fabrication and treatment

All of the bulk-heterojunction PV cells were prepared using the following device fabrication procedure. The glass/indium tin oxide (ITO) substrates [Sanyo, Japan (10 Ω/□)] were sequentially patterned lithographically, cleaned with detergent, ultrasonicated in deionized water, acetone, and isopropyl alcohol, dried on a hot plate at 120 °C for 10 min, and treated with oxygen plasma for 10 min to improve the contact angle just before film coating. Synthesized from sol–gel method, zinc oxide (ZnO) was filtered through a 0.45-μm poly(tetrafluoroethylene) (PTFE) filter before being coated on ITO by spin-coating at 3000 rpm in air, and then it was dried at 150 °C for 10 min in air. A blend of [6,6]-phenyl-C_{71}-butyric-acid methyl-ester ($PC_{71}BM$) and the polymer [1:1–1:2 (w/w)] at a concentration of 15 mg/mL in o-dichlorobenzene (o-DCB) or 1,2,4-trichlorobenzene (TCB) was stirred overnight, filtered through a 0.2-μm PTFE filter and then spin-coated (700–4000 rpm, 30 s) on top of the ZnO layer. The device was completed by the deposition of molybdenum oxide (MoO_3) and silver (Ag) layer at pressures less than 10^{-6} Torr. The active area of the device was 7 mm^2. Finally, the cell was encapsulated using UV-curing glue (Nagase, Japan).

Synthesis

All starting materials were purchased from Sigma Aldrich, Acros, Alfa Aesar or TCI and used without further purification. The following compounds were synthesized following modified literatures: benzo[2,1-b:3,4-b′]dithiophene-4,5-diones, benzo[1,2-b:4,3-b′]dithiophene-4,5-diones, 2,7-bis(trimethyltin)-4,5-(2-ethylhexyloxy)benzo[2,1-b:3,4-b′]dithiophene (BDP, **M1**) [31,32], and 4,7-bis(5-bromothiophene-2-yl)-5,6-bis(octyloxy) benzo[c][1,2,5]thiadiazole (BT, **M2**) [33].

10,13-Bis(5-bromothiophen-2-yl)-11,12-bis(octyloxy)dithieno[3,2-a:2′,3′-c]phenazine (M3)

Under a nitrogen atmosphere 4,7-bis(5-bromothiophene-2-yl)-5,6-bis(octyloxy)benzo[c] (1,2,5)-thiadiazole (**M1**, 1.44 g, 2 mmol) was dissolved in 75 mL acetic acid. Zinc powder (1.6 g, 24.8 mmol) was added in the solution. The mixture was refluxed 6 h. After cooling to room temperature, the reaction mixture was washed with a NaOH solution. The solids that resulted after the evaporation of the organic solvent and benzo[2,1-b:3,4-b′]-dithiophene-4,5-dione (1.0 g, 4.5 mmol) were dissolved in 75 mL acetic acid. The solution was refluxed for 2 days, then cooled and extracted twice with chloroform, NaOH solution. After filtration, the reaction mixture was condensed and purified by column chromatography using chloroform:hexane as the eluent (ratio 1:3) to afford 0.9 g of **M3** as a red solid (Y = 54%). ^{1}H NMR (400 MHz, ($CDCl_3$) δ): 8.52 (d, 2H, J = 5 Hz); 8.09 (d, 2H, J = 4 Hz); 7.65 (d, 2H, J = 5 Hz); 7.23 (d, 2H, J = 4 Hz); 4.12 (t, 4H, J = 7 Hz); 1.87 (m, 4H); 1.52 (m, 4H); 1.44–1.32 (m, 16H); 0.90 (m, 6H). ESI-TOF-HRMS: m/z Calcd for $[M+H]^+$ $C_{40}H_{42}Br_2N_2O_2S_4^+$, 870.8394; found 871.0770. Anal. Calcd for $C_{40}H_{42}Br_2N_2O_2S_4$ (%): C, 55.17; H, 4.86; N, 3.22; O, 3.67, S, 14.73. EA, Found (%): C, 54.11; H, 4.89; N, 3.33; O, 3.75, S, 14.65.

10,13-Bis(5-bromothiophen-2-yl)-11,12-bis(octyloxy)dithieno[2,3-a:3′,2′-c]phenazine (M4)

Under a nitrogen atmosphere 4,7-bis(5-bromothiophene-2-yl)-5,6-bis(octyloxy)benzo[c](1,2,5)thiadiazole (**M1**, 1.44 g, 2 mmol) was dissolved in 75 mL acetic acid. Zinc powder (1.6 g, 24.8 mmol)

was added in the solution. The mixture was refluxed 6 h. After cooling to room temperature, the reaction mixture was washed with a NaOH solution. The solids that resulted after the evaporation of the organic solvent and benzo[1,2-b:4,3-b′]-dithiophene-4,5-dione (1.0 g, 4.5 mmol) were dissolved in 75 mL acetic acid. The solution was refluxed for 2 days, then cooled and extracted twice with chloroform, NaOH solution. The organic phases were combined, dried over anhydrous sodium sulfate. After filtration, the reaction mixture was condensed and purified by column chromatography using chloroform:hexane as the eluent (ratio 1:3) to afford 1.0 g of **M4** as a dark red solid (Y = 60%). ^{1}H NMR (400 MHz, ($CDCl_3$) δ): 8.17 (d, 2H, J = 4 Hz); 7.89 (d, 2H, J = 5 Hz); 7.81 (d, 2H, J = 5 Hz); 7.23 (d, 2H, J = 4 Hz); 4.12 (t, 4H, J = 7 Hz); 1.87 (m, 4H); 1.52 (m, 4H); 1.44–1.32 (m, 16H); 0.90 (m, 6H). ESI-TOF-HRMS: m/z Calcd for $[M+H]^+$ $C_{40}H_{42}Br_2N_2O_2S_4^+$, 870.8355; found 870.9925. Anal. Calcd for $C_{40}H_{42}Br_2N_2O_2S_4$ (%): C, 55.17; H, 4.86; N, 3.22; O, 3.67, S, 14.73. EA, Found (%): C, 55.21; H, 4.90; N, 3.29; O, 3.72, S, 14.62.

Polymerizations

Poly[benzo[2,1-b:3,4-b′]dithiophene-thiophene-dithieno[3,2-a:2′,3′-c]phenazine] (P2)

Toluene was used as the solvent in the mixture of 2,7-bis (trimethyltin)-4,5-(2-ethylhexyloxy)benzo[2,1-b:3,4-b′]dithiophene (**M1**) (0.15 g, 0.2 mmol) and 10,13-bis(5-bromothiophen-2-yl)-11,12-bis (octyloxy)dithieno[3,2-a:2′,3′-c]phenazine (**M3**) (0.17 g, 0.2 mmol), $Pd_2(dba)_3$ (5 mg, 1 mol%), P-(o-tol)$_3$ (7 mg, 4 mol%). The mixture was heavily stirred and subjected to three successive vacuum cycles, followed by refilling with N_2 gas. The polymerization was carried out at 90 °C for 48 h. Finally, the reactant was end-capped with 2-bromothiophene and 2-tributylstannylthiophene for 8 h, respectively. The reactant then was cooled to room temperature, and the polymer was precipitated via the addition of 200 mL of methanol, filtered through a Soxhlet thimble, and then subjected to Soxhlet extraction with methanol (24 h), acetone (24 h), hexane (24 h), ethyl acetate (24 h) and chloroform (24 h). The polymer solution was condensed to ~5 mL and slowly poured into methanol (200 mL). The precipitate was collected and dried under vacuum overnight to yield **P2** (178.3 mg, 77%). GPC: M_n = 16.8 kDa, M_w = 35.9 kDa, PDI = 2.15. ^{1}H NMR (400 MHz, ($CDCl_3$) δ): 8.60–8.40 (br, 2H); 8.30–8.18 (br, 2H); 7.61–7.25 (br, 6H); 4.27–4.07 (br, 8H); 2.00–1.83 (br, 4H); 1.80–1.15 (br, 44H); 1.10–0.75 (br, 12H). Anal. Calcd for $C_{66}H_{80}N_2O_4S_6$ (%): C, 68.47; H, 6.96; N, 2.42; O, 5.53; S, 16.62. EA, Found (%): C, 67.29; H, 6.52; N, 2.29; O, 7.67; S, 12.59.

Poly[benzo[2,1-b:3,4-b′]dithiophene-thiophene-dithieno[2,3-a:3′,2′-c]phenazine] (P3)

The other polymer was synthesized in a similar manner. **P3** (171.3 mg, 74%). GPC: M_n = 40.0 kDa, M_w = 70.0 kDa, PDI = 1.75. ^{1}H NMR (400 MHz, ($CDCl_3$) δ): 8.43–8.37 (br, 2H); 8.00–7.75 (br, 6H); 7.55–7.47 (br, 2H); 4.26–4.05 (br, 8H); 2.00–1.85 (br, 4H); 1.80–1.09 (br, 44H); 1.09–0.75 (br, 12H). Anal. Calcd for $C_{66}H_{80}N_2O_4S_6$ (%): C, 68.47; H, 6.96; N, 2.42; O, 5.53; S, 16.62. EA, Found (%): C, 67.13; H, 6.50; N, 2.29; O, 7.54; S, 12.43.

Results and discussion

Molecular and thermal properties

Schemes 1 and 2 show the synthetic routes of monomers and D–π–A type polymers. One polymer (**P1**) was synthesized from our previous works and included a benzodithiophene (BDP, **M1**) derivative as a donor unit and benzothiadiazole (BT, **M2**) as an acceptor unit through the stille coupling reaction [15]. The other polymers (**P2** and **P3**) newly synthesized in this paper and included a benzodithiophene (BDP, **M1**) derivative as a donor unit and dithienophenazine (DTPz, **M3** and **M4**) derivatives as acceptor units. **P2** and **P3** were also synthesized via a palladium-catalyzed stille coupling reaction. The resulting polymers were refined in a soxhlet apparatus by sequentially using methanol, acetone, hexane, ethyl acetate and chloroform for 24 h, respectively, and they were then filtered through celite.

Finally, the chloroform fractions of **P1** and **P2** were precipitated in methanol and collected. **P1** and **P2** were quite soluble in common organic solvents, such as THF, chloroform and chlorobenzene. However, **P3** was poorly soluble in common organic solvents due to high molecular weight. So we tried to take o-DCB fraction for through the Soxhlet apparatus. The o-DCB fraction of **P3** was precipitated in methanol and collected. The color appearance of **P1**, **P2** and **P3** was violet, dark-green, and dark-green, respectively; the yields were 78%, 77% and 74%, respectively.

There are some studies on thiophene-fused conjugation structural units. When the S atom and N atom are closely located in the conjugation structure [26,28], they tend to be less soluble in

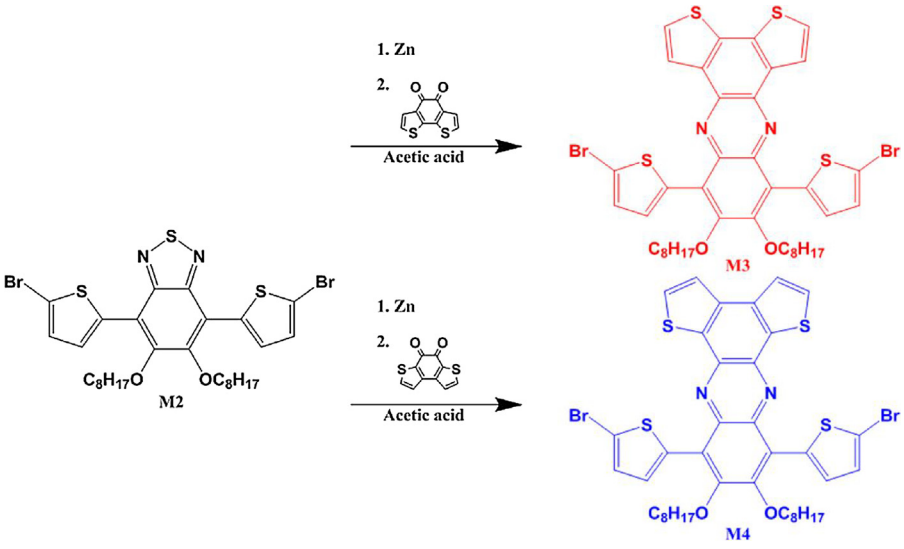

Scheme 1. Synthetic routes of monomers.

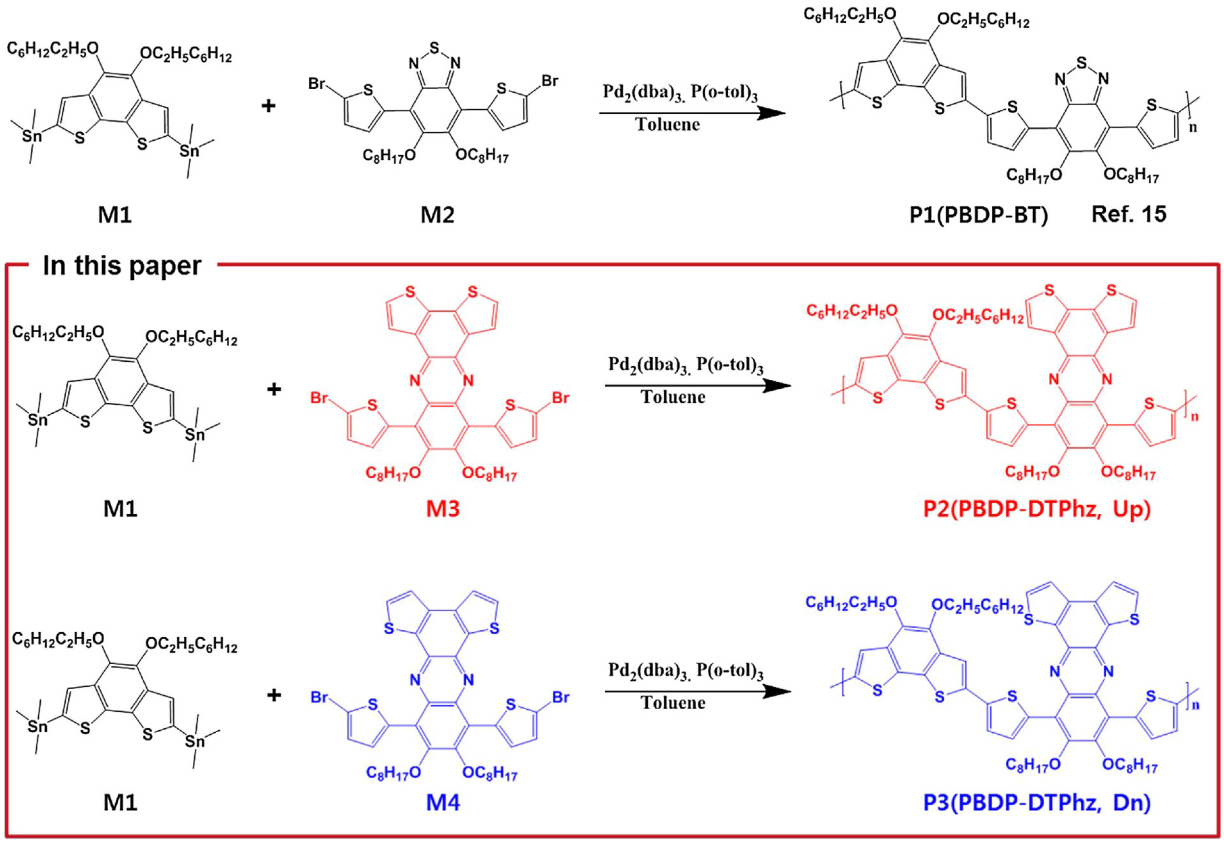

Scheme 2. Synthetic routes of polymers.

organic solvents. It means that the DTPz (dn) structure of P3 is more strong acceptor than DTPz (up) structure of P2. Thus, DTPz (dn) unit has more electronic unstable state in Pd-catalyzed stille C–C coupling reaction system (See Electronic Supporting Information, ESI, Fig. S1). The oxidative addition between brominated DTPz (dn) and Pd^0-L_n (ligand) is taken well. The C–C coupling reaction of P3 is more quickly than those of P2. As a result, P3 has a higher molecular weight and poorer solubility than P2.

The structures of the monomers and resulting polymers were identified by EA and ^{1}H NMR, and the spectra of ^{1}H NMR were especially constructed (see Figs. S2 and S3). Each monomers of the all polymers include oxygen-containing chains and contain thiophene spacers. In the structures of **P2** and **P3**, the peaks for hydrogen attached to the carbon on extended conjugation were observed at 8.6–7.3 ppm; the peak of the hydrogen attached to the carbon on thiophene spacers was 7.2–6.8 ppm; the peaks of hydrogen attached to the α and β-carbons of oxygen on the side chain were 4.3–4.0 ppm and 2.1–1.8 ppm, respectively; and the peak of the residual aliphatic protons was 1.4–0.7 ppm.

Table 1 shows the measurement results of physical and thermal properties of the obtained polymers. The number average molecular weight (Mn) of **P1**, **P2**, and **P3** corresponded to 20.4, 16.8 and 40.0 kDa, respectively. Their polydispersity indices (PDI) are 1.51, 2.14, and 1.75, respectively. The thermal stability of the polymers was measured by TGA, and the diagrams are shown in ESI (Fig. S4). All polymers showed that the temperature with 5% weight loss (T_d) under N_2 atmosphere was better than 310 °C and the three polymers were confirmed as being suitable for device fabrication and application.

Table 1
Physical and thermal properties of polymers.

	Yield [%]	Mn[a] [kDa]	Mw[a] [kDa]	PDI[a]	T_d[b] [°C]	Ref.
P1	78	20.4	30.8	1.51	312	[15]
P2	77	16.8	35.9	2.14	334	–
P3	74	40.0	70.0	1.75	334	–

[a] Determined by GPC in chloroform using polystyrene standards.
[b] Temperature resulting in 5% weight loss based on the initial weight.

Optical properties

Fig. 1 shows the UV–vis absorption spectra (Fig. 1, (a): diluted chloroform solution, (b): thin film) of polymers. The results are shown in Table 2. The absorption peaks (λ_{max} = 300–500 nm) of **P1**, **P2** and **P3** polymers through delocalized π–π* transitions were 400 nm, 411 nm and 440 nm. The molecular absorption coefficient (ε) of polymers in solution state was calculated as $2.8 \times 10^4\ M^{-1}\ cm^{-1}$, $3.9 \times 10^4\ M^{-1}\ cm^{-1}$ and $3.8 \times 10^4\ M^{-1}\ cm^{-1}$, respectively.

Polymers containing DTPz derivatives as acceptors showed higher intensity on π–π* transition effects than polymers containing BT. However, regarding the absorption peak (λ_{max} = 500–750 nm) by the intermolecular charge transfer (ICT) effects between donor and acceptor units, **P1** showed higher intensity than **P2** and **P3**. These results correspond to the results of Wood et al. who reported that polymers, comprised of BT and thiophene, showed higher intensity at the long-wavelength range [16].

The UV–vis absorption spectra of these polymers were similar to the properties of acceptor monomers (see Fig. S5). In regard to DTPz (M3 and M4), specifically M4 monomers where the S atom is located closer to the N atom tended to show a greater red-shift property [22,23,30].

The UV–vis absorption spectra of the polymer films were 26 nm, 45 nm and 18 nm more red-shifted than in the solution

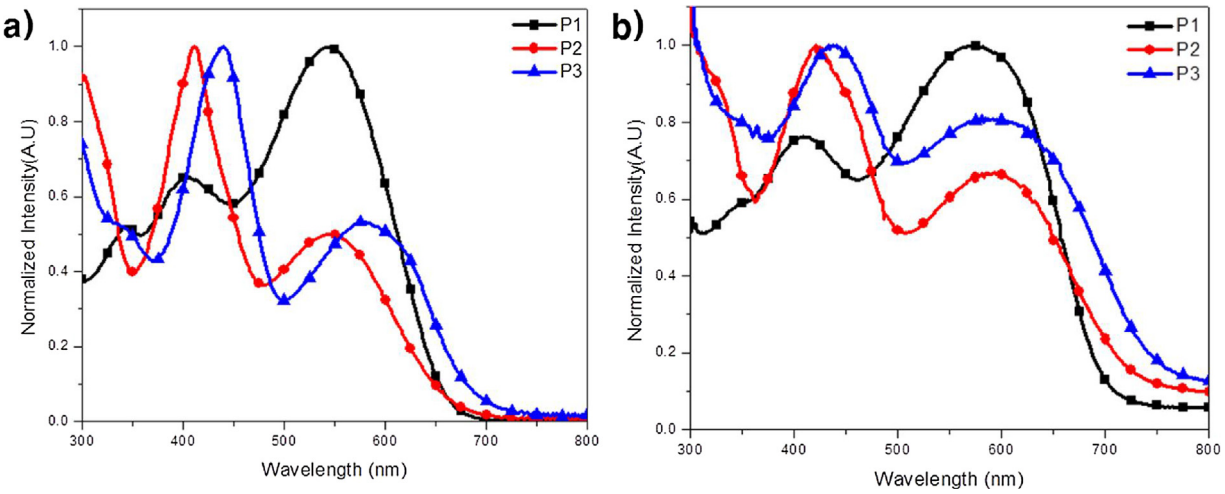

Fig. 1. Normalized UV–vis absorption spectra of polymers in (a) solution and (b) film.

Table 2
Optical and electrochemical properties of polymers.

	UV–vis absorption				$E_g^{opt,a}$ [eV]	Cyclic voltammetry		Ref.
	$CHCl_3$ solution		Film			HOMO[b] [eV]	LUMO[a] [eV]	
	λ_{max} [nm]	ε at λ_{max} [M^{-1} cm^{-1}]	λ_{max} [nm]	λ_{onset} [nm]				
P1	400, 546	42,500	409, 572	678	1.83	−5.31	−3.48	[15]
P2	411, 548	38,700	421, 593	718	1.72	−5.30	−3.58	–
P3	440, 578	38,000	441, 596	746	1.66	−5.29	−3.63	–

[a] Calculated from the intersection of the tangent on the low energetic edge of the absorption spectrum with the baseline.
[b] $E_{HOMO\ (or\ LUMO)} = -[E_{onset}(vs\ Ag/AgCl) - E_{1/2}(Fc/Fc^{+}\ vs\ Ag/AgCl)] - 4.8\ eV$.

state. This implies that the polymer main chain shows stronger aggregation and more ordered π–π stacking in the film state than in the solution state [24,30]. Thus, the polymers induced a more effective ICT transition and showed red-shift properties in the film state [34,35]. Furthermore, **P2** and **P3** absorbed a broader range of photons, and showed a decrease in band-gap by 0.11–0.17 eV (1.83 eV → 1.66 eV).

Electrochemical properties

The electronic energy level of polymers was measured using cyclic voltammetry (CV), and the results are shown in Fig. 2 and Table 2. As shown in Table 2, the HOMO levels of the three polymers were calculated as −5.31 eV, −5.30 eV and −5.29 eV. The LUMO level was calculated by the difference between the HOMO

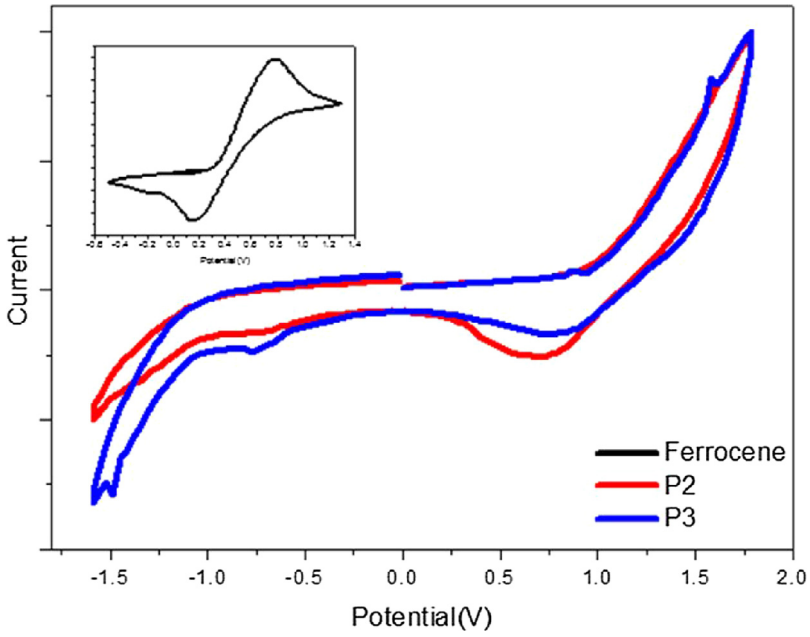

Fig. 2. Cyclic voltammograms of polymers and reference (Fc/Fc+).

Table 3
Calculated parameters of polymers.

	Dihedral angle (deg)			HOMO [eV]	LUMO [eV]	Ref.
	θ_1	θ_2	θ_3			
P1	8.4	14.9	18.7	−4.99	−2.55	[15]
P2	0	22.5	27.0	−5.00	−2.50	–
P3	0	19.2	27.0	−4.99	−2.56	–

level and the optical band gap (E_g^{opt}), and the LUMO levels were −3.51 eV, −3.58 eV and −3.63 eV. The polymers showed similar HOMO levels due to the presence of the same donor unit, and LUMO levels changed due to the difference in acceptor units [20,30].

Theoretical calculations

Density functional theory (DFT) was used to calculate electrical properties; electron density of states distribution; molecular geometries; and dihedral angles of polymers. For DFT calculations, Gaussian 09 was used as the hybrid B3LYP correlation functional and split valence 6-31G(d) basis set. For computational simplicity, the calculations were carried by simplifying the polymer backbones as oligomers with one repeated unit and alkoxy chain with methoxy being one. Calculated HOMO and LUMO orbitals and their geometries are indicated in Fig. 2; the dihedral angle and energy level of the main chain are shown in Table 3.

Fig. 3(a) indicates optimized geometries at the front of the polymer backbone. The angle (θ_1) between the BDP unit and the thiophene in the all three polymers less than 10°. However, when the structure was changed from containing a BT unit to DTPz, the angles (θ_2, θ_3) between the acceptor unit and thiophene were 14.9°, 18.7° (**P1**), whereas the angles were increased to 22.5°, 27.0° (**P2**) and 19.2°, 27.0° (**P3**). This difference is because the bulk structure increased steric hindrance, thereby reducing the planarity of the polymers. Nevertheless, the θ_2 of **P3** is lower than those of **P2** because the dn structure of **P3** has a strong intermolecular interaction.

Fig. 3(b, c) shows energy levels of calculated polymers from DFT results. The calculated energy levels of **P1**, **P2** and **P3** are showing similar HOMO values due to the same electron donating group. However, **P3** due to the S atom was located near the N atom showed a deeper LUMO level than **P2**. As shown in Fig. 2, the HOMO orbitals of three polymers were delocalized at the polymer backbone, and in their LUMO orbitals, their electron clouds are localized at the acceptor units with a spacer. These results were caused by the quinoid structural unit [10,36] by non-bonding electron pairs located between the N atom and the S atom of the BT and DTPz units.

XRD measurement

X-ray diffraction was measured to analyze the ordering structure of the polymers. Fig. 4 indicates the X-ray diffraction of thin film polymers in the out-of-plane mode (a) and in-plane mode (b).

When measured in the out-of-plane mode, a definite (100) peak (5.6°, 15.87 Å) was confirmed at a low angle for **P1**. However, at the high angle showing the (010) peak, **P1**, **P2** and **P3** showed broader peaks (20.5°, 21.9° and 22.0°, respectively). The intermolecular π–π stacking distances (d_π), calculated with these measurements, were 4.34 Å, 4.06 Å and 4.04 Å, respectively.

Likewise, if π–π stacking peak is observed in the out-of-plane mode with (010) peak, crystallite has a high probability of forming with a face-on orientation in the thin film polymer, which can be confirmed by X-ray diffraction in the in-plane mode. All polymers, when measured in-plane mode, did not showed any peak at a low angle. This implies that all polymers have a face-on orientation. The face-on orientation of polymers allows effective charge transfer in the perpendicular direction.

Fig. 5 explains why all the polymers formed with face-on orientation. In terms of the monomer, BT and DTPz units have an

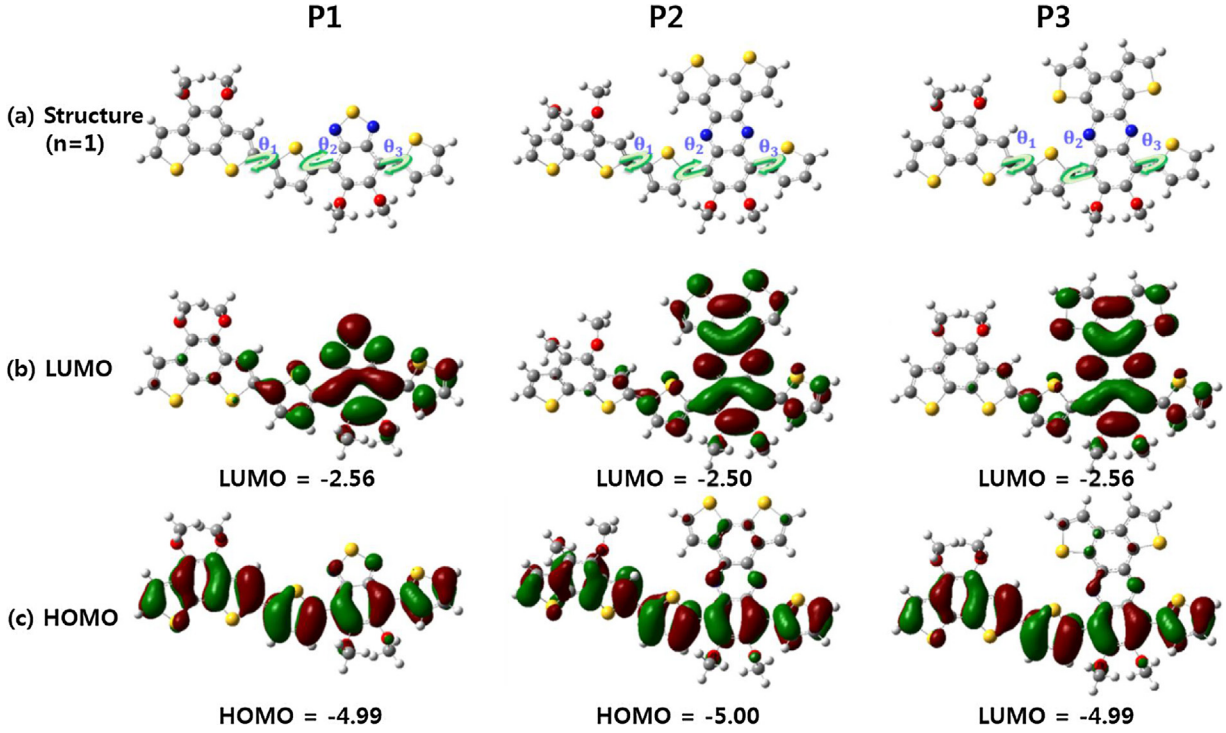

Fig. 3. Top view of the optimized geometries of the backbone of polymers n = 1 (a), LUMO (b) and HOMO (c); color code: gray (C), white (H), red (O), blue (N) and yellow (S). Energy levels of calculated polymers from DFT. (For interpretation of the references to color in this figure legend, the reader is referred to the web version of this article.)

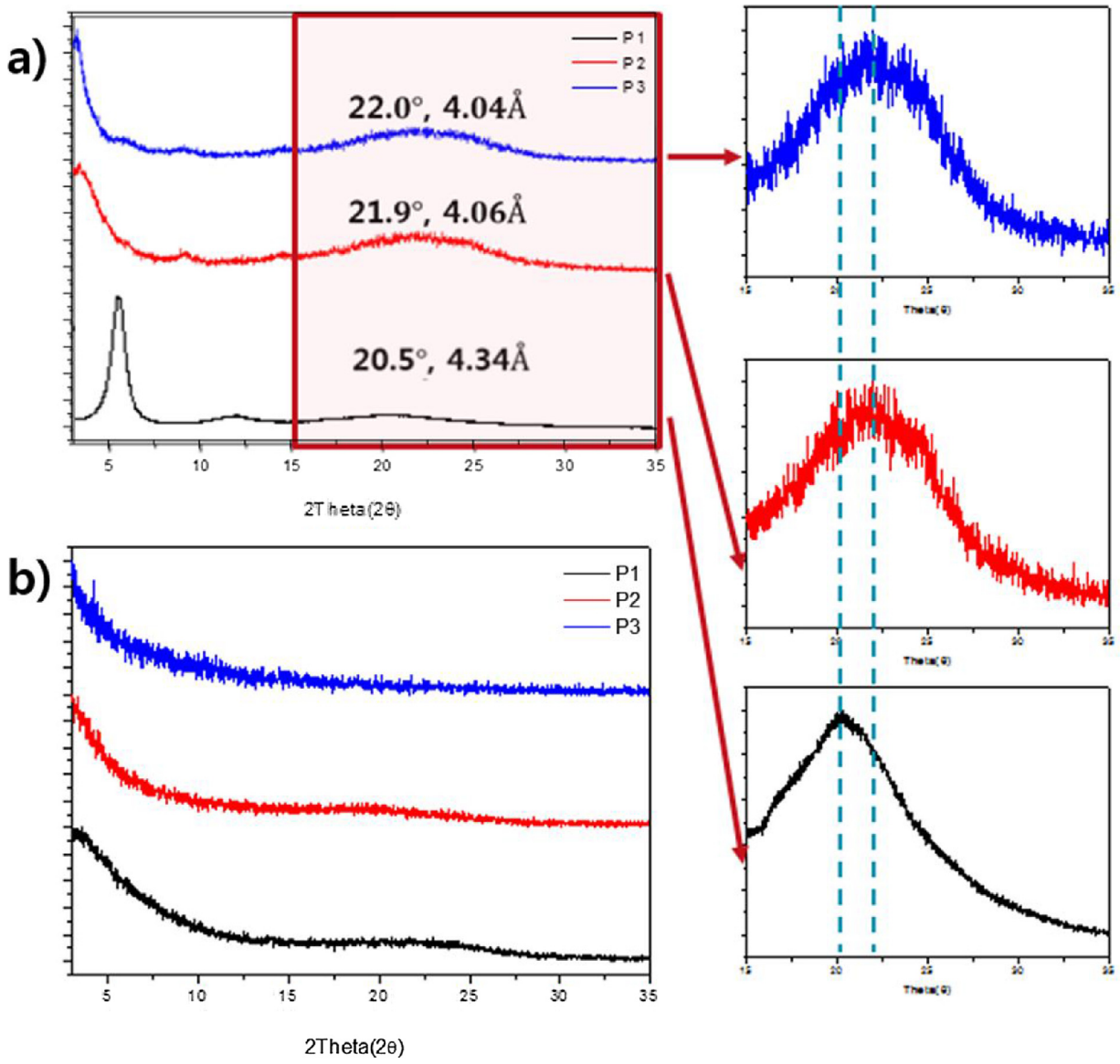

Fig. 4. X-ray diffraction pattern of polymers on a silicon wafer (a) out-of-plane mode and (b) in-plane mode.

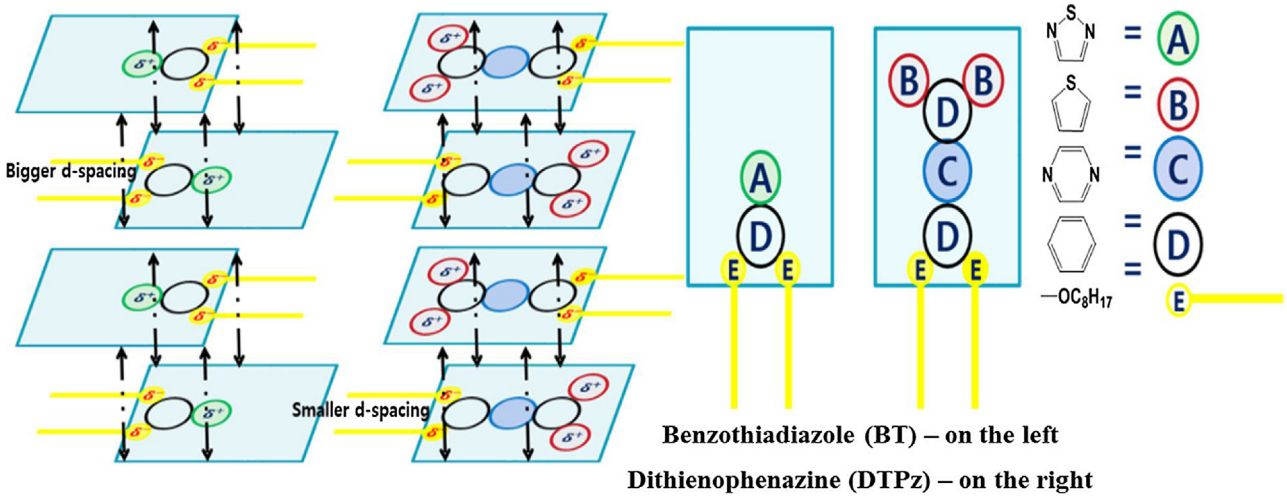

Fig. 5. Non-covalent interactions on molecular stacking between asymmetric acceptors.

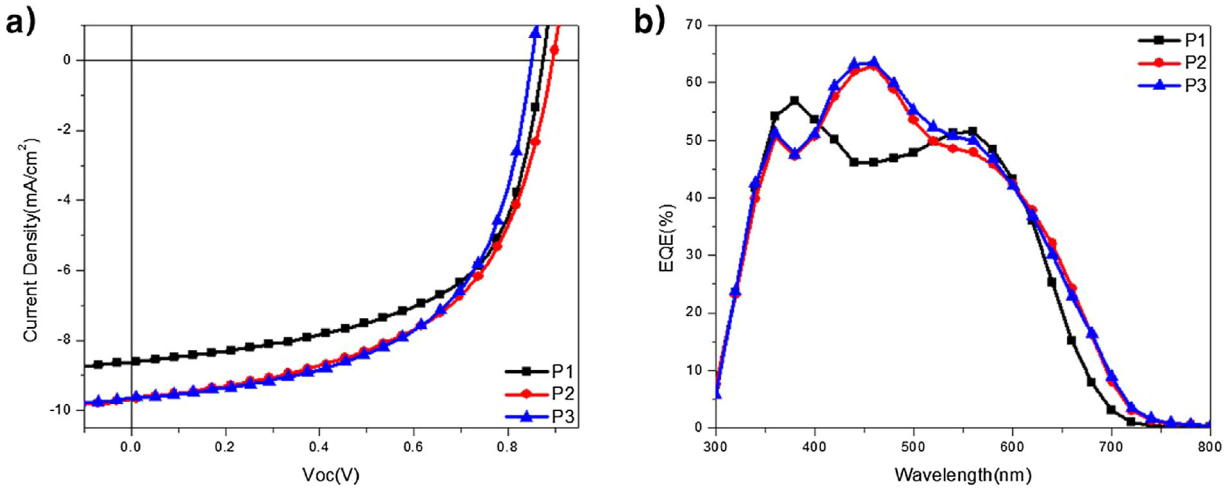

Fig. 6. (a) The J–V curves of the OPVs based on polymer:$PC_{71}BM$ under the illumination of AM 1.5G, 100 mW/cm^2. (b) The external quantum efficiency of the OPVs based on polymer:$PC_{71}BM$.

asymmetric structure, with S, N and O atoms at the top, center and bottom, respectively. In this case, intermolecular packing leads to repulsion between the same atoms. Thus, reverse stacking becomes more stable. Furthermore, an alternately stacked structure induces non-covalent interactions looks like dipole–dipole interaction due to difference in electronegativity of hetero atoms (see Fig. S6). As a result, a narrower molecular stacking can form. The same effect is applicable to polymers, where the face-on orientation is dominant [36–44].

P2 and **P3** containing the DTPz units had the same numbers of S atoms and O atoms. Thus, the non-covalent interactions became more effective, and the face-on orientation allowed clearer and closer molecular stacking. Therefore, **P2** and **P3** were expected to exhibit effective charge transfer.

Photovoltaic properties and morphology analysis

Inverted-structure devices were fabricated to confirm the photovoltaic properties of the obtained polymers. The properties were evaluated after OPV devices having the structure of ITO/ZnO/polymer:$PC_{71}BM$/MoO_3/Ag were fabricated and encapsulated in a glove box. The weight ratio of polymer:$PC_{71}BM$ showed the best efficiency when measured at 1:1.5 (w/w). o-DCB was used as the solvent for **P1** and **P2**; TCB was used as the solvent for **P3** due to its lower solubility.

Fig. 6(a) shows the J–V curves of the photovoltaic device at the ratios of polymer and $PC_{71}BM$ (1:1.5). Fig. 6(b) shows the IPCE spectra of those devices. Detailed data are shown in Table 4.

Three polymers showed the best performance when **P1**, at Jsc = 8.5 mA/cm^2, Voc = 0.88 V, FF = 57.7% and with PCE = 4.3%; **P2**, at Jsc = 9.7 mA/cm^2, Voc = 0.90 V, FF = 54.4% and with PCE = 4.8%; and **P3**, at Jsc = 9.7 mA/cm^2, Voc = 0.86 V, FF = 56.4% and with PCE = 4.7%. **P2** and **P3** showed relatively higher PCE than **P1**. Voc is determined by the difference between the HOMO energy level of a polymer and the LUMO energy level of $PC_{71}BM$; the HOMO levels of D–A-type polymers are determined by BDP, the donor unit. The HOMO levels of the three polymers by CV measurement and DFT calculation had similar values; thus, the Voc of the three polymers must have similar values. However, **P3** showed low Voc due to non-uniform surface properties, as Chen reported [45].

Table 4
Photovoltaic devices performances of polymers:$PC_{71}BM$ (1:1.5).

	Voc [V]	Jsc [mA cm^{-2}]	FF [%]	PCE [%]	Jsc at IPCE [mA cm^{-2}]	Ref.
P1	0.88	8.5	57.7	4.3	8.03	[15]
P2	0.90	9.7	54.7	4.8	8.97	–
P3	0.86	9.7	56.4	4.7	9.11	–

The Jsc values of **P2** and **P3** increased by 14.1% due to a broad absorption range and molecular stacking. External quantum efficiency (EQE) was measured to test the accuracy of the Jsc measurement. These devices showed high EQE values in the absorption range of 300–600 nm and showed low EQE values above 600 nm. Furthermore, **P2** and **P3** have higher EQE_{max} values of greater than 60%; however, **P1** showed lower EQE_{max} of 50%.

Morphology

The morphologies of polymer:$PC_{71}BM$ blend films were confirmed via atomic force microscopy (AFM), as shown in Fig. 7. Dark-colored and light-colored areas correspond to $PC_{71}BM$ domains and polymers, respectively. The surfaces of **P1**:$PC_{71}BM$ and **P2**:$PC_{71}BM$ blended films have smooth nanoscale features, showing small root-mean-square (RMS) roughness values of 0.63 and 0.43 nm, respectively.

Inter-mixing of polymers and $PC_{71}BM$ is frequent, allowing frequent channel formation [14,29]. In particular, **P1** has a higher RMS than **P2**; however, the nano-fibril structure of **P1** was confirmed in the phase image, which enhanced FF [46,47].

On the other hand, a rough surface of **P3**:$PC_{71}BM$ blend film was confirmed with a RMS roughness of 1.18 nm. **P3** had higher RMS roughness because **P3** is less soluble in organic solvent and thereby had difficulty forming a uniform film.

Hole mobility measurement

The hole mobility was measured by the space charge limited current (SCLC) method in the hole-only devices with a device structure of ITO/PEDOT:PSS/polymer:$PC_{71}BM$/MoO_3/Ag, and the Mot–Gurney space charge limited current formula [eqn. $J = (9/8)\varepsilon_0\varepsilon_r\mu((V^2)/(d^3))$, where J is the current, μ is the zero-field mobility, ε_0 is the permittivity of free space, ε_r is the relative permittivity of the material, d is the thickness of the active layer, and V is the effective voltage.] was used to calculate the mobility. The hole mobility of the **P1**, **P2** and **P3** was 1.64×10^{-4} cm^2 V^{-1} s^{-1}, 5.61×10^{-4} cm^2 V^{-1} s^{-1} and 3.59×10^{-4} cm^2 V^{-1} s^{-1} (see Fig. S7 and

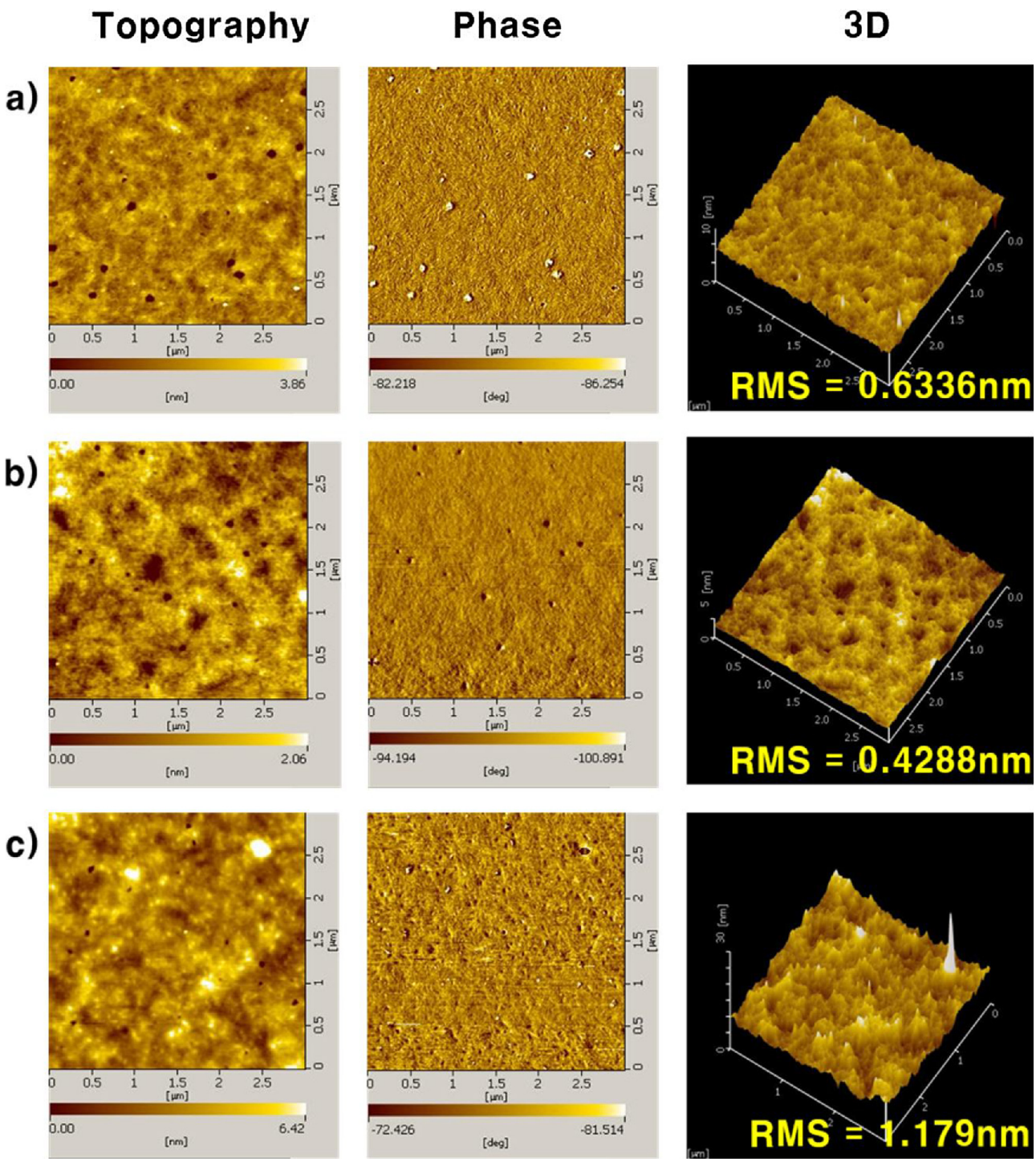

Fig. 7. Topographic AFM images ($3 \times 3\ \mu m^2$) of (a) **P1**: $PC_{71}BM$ = 1:1.5, (b) **P2**: $PC_{71}BM$ = 1:1.5, (c) **P3**: $PC_{71}BM$ = 1:1.5.

Table S1). Specifically, **P2** and **P3** had a high hole mobility than those of **P1** due to closer molecular stacking. The results proved that **P2** and **P3** had a high Jsc than those of P1 [48].

Conclusions

DTPz units were synthesized to extend conjugated system compared to BT unit and to increase the number of S atoms. BT and DTPz units were having non-covalent interactions due to their structural properties and showing a packing property with dominant face-on orientation. Specifically, in polymers containing the DTPz units, absorption spectra were red-shifted to the long wavelength, and narrow π–π stacking distances were observed than those of **P1**. Thus, the Jsc values of **P2** and **P3** were enhanced in the fabrication of OPVs. The DTPz units had two isomers, in accordance with the position of the S atom in the fused thiophene. **P3** with S atom facing toward the main chain has an extended absorption spectrum; however, the S atom had a rough morphology due to high aggregation. On the other hand, **P2** with S atom pointing away from the main chain resulted in good solubility in

organic solvents despite the similar optical and stacking properties of **P3**. Thus, **P2** with $PC_{71}BM$ in optimized condition is achieved the best PCE of 4.8%; Voc, Jsc and FF were 0.9 V, 9.7 mA/cm^2, and 54.4%, respectively.

Acknowledgments

This research was supported by the New & Renewable Energy Core Technology Program (No. 20153010140030) and Human Resources Program in Energy Technology (No. 20174010201540) of the Korea Institute of Energy Technology Evaluation and Planning (KETEP) grant funded by the Ministry of Trade, industry & Energy, Republic of Korea.

Appendix A. Supplementary data

^{1}H NMR spectra of polymers, TGA data of polymers, UV absorption spectra of monomers. Supplementary data associated with this article can be found, in the online version, at 10.1016/j.jiec.2018.02.015

References

[1] S.C. Cevher, G. Hizalan, C. Temiz, Y.A. Udum, L. Toppare, A. Cirpan, Polymer 101 (2016) 208.
[2] L. Dou, J. You, Z. Hong, Z. Xu, G. Li, R.A. Street, Y. Yang, Adv. Mater. 25 (2013) 6642.
[3] J. Zhao, Y. Li, G. Yang, K. Jiang, H. Lin, H. Ade, W. Ma, H. Yan, Nat. Energy 1 (2016) 15027.
[4] E. Salatelli, T. Benelli, D. Caretti, V. Cocchi, L. Giorgini, M. Lanzi, L. Mazzocchetti, Polymer 97 (2016) 314.
[5] Q. Gan, F.J. Bartoli, Z.H. Kafafi, Adv. Mater. 25 (2013) 2385.
[6] T. Wang, A.J. Pearson, D.G. Lidzey, J. Mater. Chem. C 1 (2013) 7266.
[7] P. Morvillo, R. Diana, C. Fontanesi, R. Ricciardi, M. Lanzi, a. Mucci, F. Tassinari, L. Schenetti, C. Minarini, F. Parenti, Polym. Chem. 5 (2014) 2391.
[8] A.J. Heeger, Adv. Mater. 26 (2014) 10.
[9] F. Peng, B. Zhao, J. Xu, Y. Zhang, Y. Fang, R. He, H. Wu, W. Yang, Y. Cao, Org. Electron. 29 (2016) 151.
[10] M.-H. Choi, K.W. Song, D.K. Moon, Polym. Chem. 6 (2015) 2636.
[11] Q. Fan, Y. Liu, M. Xiao, H. Tan, Y. Wang, W. Su, D. Yu, R. Yang, W. Zhu, Org. Electron. Phys. 15 (2014) 3375.
[12] Q. Fan, Y. Liu, M. Xiao, W. Su, H. Gao, J. Chen, H. Tan, Y. Wang, R. Yang, W. Zhu, J. Mater. Chem. C 3 (2015) 6240.
[13] Y. Zhang, J. Zou, H.L. Yip, K.S. Chen, D.F. Zeigler, Y. Sun, A.K.Y. Jeni, Chem. Mater. 23 (2011) 2289.
[14] R. He, L. Yu, P. Cai, F. Peng, J. Xu, L. Ying, J. Chen, W. Yang, Y. Cao, Macromolecules 47 (2014) 2921.
[15] T.H. Lee, M.H. Choi, S.J. Jeon, D.K. Moon, Polymer 99 (2016) 756.
[16] S. Wood, J.-H. Kim, J. Wade, J.B. Park, D.-H. Hwang, J.-S. Kim, J. Mater. Chem. C 4 (2016) 7966.
[17] G. Li, Z. Lu, C. Li, Z. Bo, Polym. Chem. 6 (2015) 1613.
[18] Q. Fan, X. Xu, Y. Liu, W. Su, X. He, Y.-M. Zhang, H. Tan, Y. Wang, Q. Peng, W. Zhu, Polym. Chem. 8 (2016) 1747.
[19] H.J. Song, T.H. Lee, M.H. Han, J.Y. Lee, D.K. Moon, Polymer 54 (2013) 1072.
[20] Y. Lee, Y.M. Nam, W.H. Jo, J. Mater. Chem. 21 (2011) 8583.
[21] Z. Guo, T. Lei, Z. Jin, J. Wang, J. Pei, Org. Lett. 15 (2013) 3530.
[22] Y. Xie, T. Fujimoto, S. Dalgleish, Y. Shuku, M.M. Matsushita, K. Awaga, J. Mater. Chem. C 1 (2013) 3467.
[23] C.A. Richard, Z. Pan, A. Parthasarathy, F.A. Arroyave, L.A. Estrada, K.S. Schanze, J. R. Reynolds, J. Mater. Chem. A 2 (2014) 9866.
[24] J. Kesters, P. Verstappen, W. Vanormelingen, J. Drijkoningen, T. Vangerven, D. Devisscher, L. Marin, B. Champagne, J. Manca, L. Lutsen, D. Vanderzande, W. Maes, Sol. Energy Mater. Sol. Cells 136 (2015) 70.
[25] Y. Zhang, J. Zou, H.-L. Yip, K.-S. Chen, J. Davies, Y. Sun, A. Jen, Macromolecules 44 (2011) 4752.
[26] J. Zhang, W. Cai, F. Huang, E. Wang, C. Zhong, S. Liu, M. Wang, C. Duan, T. Yang, Y. Cao, Macromolecules 44 (2011) 894.
[27] A. Putta, J.D. Mottishaw, Z. Wang, H. Sun, Cryst. Growth Des. 14 (2014) 350.
[28] T.L. Nguyen, S. Xu, S. Hwang, C.E. Park, H.Y. Woo, Chem. Mater. 26 (2014) 2147.
[29] M.A. Uddin, T.H. Lee, S. Xu, S.Y. Park, T. Kim, S. Song, T.L. Nguyen, S.J. Ko, S. Hwang, J.Y. Kim, H.Y. Woo, Chem. Mater. 27 (2015) 5997.
[30] R. Mondal, H.a. Becerril, E. Verploegen, D. Kim, J.E. Norton, S. Ko, N. Miyaki, S. Lee, M.F. Toney, J.-L. Brédas, M.D. McGehee, Z. Bao, J. Mater. Chem. 20 (2010) 5823.
[31] Y. a. Getmanenko, M. Fonari, C. Risko, B. Sandhu, E. Galán, L. Zhu, P. Tongwa, D. K. Hwang, S. Singh, H. Wang, S.P. Tiwari, Y.-L. Loo, J.-L. Brédas, B. Kippelen, T. Timofeeva, S.R. Marder, J. Mater. Chem. C 1 (2013) 1467.
[32] A. Meyer, E. Sigmund, F. Luppertz, G. Schnakenburg, I. Gadaczek, T. Bredow, S.S. Jester, S. Höger, Beilstein J. Org. Chem. 6 (2010) 1180.
[33] M.H. Choi, K.W. Song, S.W. Heo, Y.W. Han, D.K. Moon, J. Ind. Eng. Chem. 26 (2014) 173.
[34] X. Lu, T. Lan, Z. Qin, Z.S. Wang, G. Zhou, ACS Appl. Mater. Interfaces 6 (2014) 19308.
[35] S. Li, B. Zhao, Z. He, S. Chen, J. Yu, A. Zhong, R. Tang, H. Wu, Q. Li, J. Qin, Z. Li, J. Mater. Chem. A 1 (2013) 4508.
[36] M.-H. Choi, H.Y. Kim, E.J. Lee, D. Kyung Moon, Polymer 91 (2016) 162.
[37] H. Heo, H. Kim, D. Lee, S. Jang, L. Ban, B. Lim, J. Lee, Y. Lee, Macromolecules 49 (2016) 3328.
[38] A.M. Maharramov, K.T. Mahmudov, M.N. Kopylovich, A.J.L. Pombeiro (Ed.), John Wiley & Sons Inc., Hoboken, NJ, 2016, p. 1.
[39] K.T. Mahmudov, A.J.L. Pombeiro, Chem. Eur. J. 22 (2016) 16356.
[40] K.T. Mahmudov, M.N. Kopylovich, M.F.C. Guedes da Silva, A.J.L. Pombeiro, Coord. Chem. Rev. 345 (2017) 54.
[41] K.T. Mahmudov, M.N. Kopylovich, M.F.C. Guedes da Silva, A.J.L. Pombeiro, Dalton Trans. 46 (2017) 10121.
[42] B. Kim, H.R. Yeom, M.H. Yun, J.Y. Kim, C. Yang, Macromolecules 45 (2012) 8658.
[43] A.K. Mahrok, E.I. Carrera, A.J. Tilley, S. Ye, D.S. Seferos, Chem. Commun. 51 (2015) 5475.
[44] M. Planells, B.C. Schroeder, I. McCulloch, Macromolecules 47 (2014) 5889.
[45] W. Chen, Z. Du, L. Han, M. Xiao, W. Shen, T. Wang, Y. Zhou, R. Yang, J. Mater Chem. A 3 (2015) 3130.
[46] F. Pierini, M. Lanzi, P. Nakielski, S. Pawlowska, O. Urbanek, K. Zembrzycki, T.A. Kowalewski, Macromolecules 50 (2017) 4972.
[47] J.J.V. Franeker, M. Turbiez, W. Li, M.M. Wienk, R.A.J. Janssen, Nat. Commun. 6 (2017) 6229.
[48] K. Feng, G. Yang, X. Xu, G. Zhang, H. Yan, O. Awartani, L. Ye, H. Ade, Y. Li, Q. Peng, Adv. Energy Mater. (2017)1602773.